research papers

Structures and thermal stability of the α-LiNH₄SO₄ polytypes doped with Er^{3+} and Yb^{3+}

N. P. Sabalisck,[a]* C. Guzmán-Afonso,[a] C. González-Silgo,[a] M. E. Torres,[a] J. Pasán,[a,b] J. del-Castillo,[a] D. Ramos-Hernández,[a] A. Hernández-Suárez[a] and L. Mestres[c]

[a]Departamento de Física, Facultad de Ciencias, Sección Física, Universidad de La Laguna, 38206 La Laguna, Tenerife, Spain, [b]Institut de Ciencia Molecular (ICMol), C/ Catedrático José Beltrán 2, 46980 Paterna, Valencia, Spain, and [c]Grup de Química de l'Estat Sòlid, Departament de Química Inorgànica, Universitat de Barcelona, 08028 Barcelona, Spain. *Correspondence e-mail: nanprado@ull.edu.es

In order to clarify the polymorphism in the lithium sulfate family, $LiRE_x(NH_4)_{1-x}SO_4$ ($0.5 \leq x \leq 4.0$ mol%, nominal value; RE = Er^{3+}, Yb^{3+} and Dy^{3+}) crystals were grown from aqueous solution by slow evaporation between 298 and 313 K. The doping of the samples allowed us to obtain two polymorphic forms, α and β, of $LiNH_4SO_4$ (LAS). By means of X-ray diffraction (XRD) in single crystals, we determined the crystal structures of two new α-polytypes, which we have named α_1- and α_2-LAS. They present the same space group $P2_1/c$ and the following relation among their lattice parameters: $a_2 = -c_1$, $b_2 = -b_1$, $c_2 = -2a_1 - c_1$. In order to evaluate the stability of the new α-polytypes, we performed thermal analysis, X-ray diffraction and dielectric spectroscopy on single crystals and polycrystalline samples over the cyclic temperature range: $190 \rightarrow 575 \rightarrow 190$ K. The results obtained by all the techniques used in this study demonstrate that α-polytypes are stable across a wide range of temperatures and they show an irreversible phase transition to the paraelectric β-phase above 500 K. In addition, a comparative study of α- and β-polytypes shows that both polymorphic structures have a common axis, with a possible intergrowth that facilitates their coexistence and promotes the reconstructive $\alpha \rightarrow \beta$ transition. This intergrowth was related to small anomalies detected between 240 and 260 K, in crystals with an α-habit.

1. Introduction

In the last few years, considerable attention has been devoted to the lithium sulfate family with the chemical formula $ALiSO_4$ (A = Li, Na, K, Rb, Cs, NH₄ or Tl) and related compounds. These materials present open lattices, which provide them with a great flexibility that makes possible thermal rearrangements of their LiO_4 and SO_4 tetrahedra, involving phase transitions (Tomaszewski, 1992b; Połomska, 2001; Mata-Ramírez, 2002; Lim et al., 2013, and references cited therein). This ability to generate polymorphism allows a large number of different crystal structures to be obtained, which display interesting nonlinear physical properties of current interest such as ferroelectricity (Połomska et al., 2005; Shamshin, 2010), ferroelasticity (Czaja, 2013; Lim & Kim, 2012) and second harmonic generation (Palmero et al., 2008; Closser et al., 2013); as well as fast-ion conduction at higher temperatures (Lv et al., 2015; Xiao et al., 2015). In the case of the lithium ammonium sulfate (LAS), its varied polymorphism and its phase transition sequence (which depend on the synthesis conditions, i.e. thermal treatment, doping of the ammonium ion etc.), have been the subject of more than 200 articles in the last 50 years, which were not exempt from

1mm
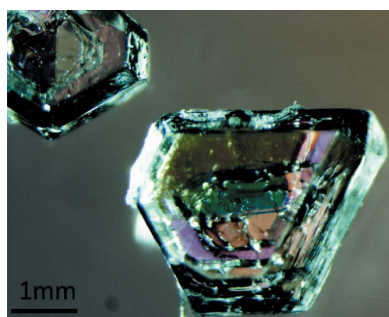
controversy (for instance, see Solans *et al.*, 1999; Tomaszewski, 2000). Still nowadays some phases are being revised and referenced (Komornicka *et al.*, 2014; Rudysh *et al.*, 2015; Lim, 2016). Moreover, a variety of phases in this family is largely influenced by the chemical pressure, which can be changed by the replacement of cations and anions (Połomska, 2001; Lim *et al.*, 2013; Czaja, 2013; Rousse & Tarascon, 2014).

The three polymorphic phases and thermal stability of β-LiNH$_4$SO$_4$ (β-LAS) have been described as: ferroelectric β-LAS, from 285 to 460 K ($P2_1cn$ space group; Połomska, 2001). Above 460 K the corresponding ferroelectric–paraelectric transition to a crystal structure with the space group $Pmcn$ takes place (Itoh *et al.*, 1981). Below 285 K, it undergoes a ferroelectric–ferroelastic phase transition with a final mono-clinic phase ($P2_1/c$; Mashiyama & Kasano, 1993). Very recently, this non-polar and ferroelastic phase has been iden-tified as a ferroaxial crystal structure (Hlinka *et al.*, 2016). There is also the so-called α-LiNH$_4$SO$_4$ (α-LAS) or α-modi-fication. It has been described as an orthorhombic structure with the space group $Pbc2_1$ and the following lattice para-meters: $a = 4.991$, $b = 10.196$ and $c = 17.010$ Å ($Z = 8$; Pietraszko & Lukaszewicz, 1992; Tomaszewski, 1992*a*). The α-modification presents a complex correlated structural disorder that can be represented by, at least, three different polytypes and whose lattice parameters c follow the conditions: $c_1 = c$, $c_2 = 2c$ and $c_3 = 3c$ (Tomaszewski, 1992*a*). Recently, Komor-nicka *et al.* (2014) have studied the polytypism in α-LAS. They have simulated the X-ray diffuse scattering by the Monte Carlo technique, using a two-spin like Ising model of disorder. This model incorporates correlations into the α-polytypism, described as a 'domainized' sequence of layers.

Several authors have studied the growth conditions, thermal stability and phase transitions of both modifications: α- and β-LAS. The crystallization above and at room temperature favors the ferroelectric β-phase, whereas the α-polytype is obtained below room temperature (Solans *et al.*, 1999; Połomska, 2001; Mel'nikova *et al.*, 2003). According to the literature, the α-LAS modification has an unstable structure and undergoes a reversible phase transition to β-LAS at 250 K and a non-reversible phase transition to the ferroelectric phase of β-LAS, at ~ 350 K (Połomska, 2001). Another study of crystal growth conditions of α- and β-LAS performed by Mel'nikova *et al.* (2003) showed that there are two tempera-ture intervals where the crystal may experience a recon-structive $\alpha \rightarrow \beta$ phase transition. In the first temperature interval (340–350 K) a reconstructive phase transition causes the fast destruction of the sample. In the second temperature interval (440–450 K) the crystal structure undergoes a slow transformation (recrystallization) without significant distor-tions. Using XRD, Komornicka *et al.* (2014) confirmed the reconstructive and irreversible $\alpha \rightarrow \beta$ phase transition between 431 and 457 K.

In this work we present two new crystal structures of Yb^{3+}-doped LiNH$_4$SO$_4$, obtained from XRD of single crystals, which are new polytypes of the α-LAS modification. In addition, from DSC and dielectric spectroscopy of single crystals and XRD of polycrystalline samples, we study the

Table 1
Concentrations of Er^{3+}, Yb^{3+} and Dy^{3+} used to obtain doped LiNH$_4$SO$_4$ crystals.

| Rare earth	Nominal concentration (mol%)									
Er^{3+}	–	0.6	–	0.8	–	1.0	1.2	1.4	2.0	–
Yb^{3+}	0.5	0.6	0.7	0.8	0.9	1.0	1.2	1.4	2.0	4.0
Dy^{3+}	–	0.6	–	0.8	–	1.0	1.2	–	–	–

thermal stability, the reconstructive $\alpha \rightarrow \beta$ phase transition and the possible coexistence of both α and β polymorphs for different Yb^{3+} and Er^{3+} doped samples with α modification. In this study we try to clarify most of the controversy given in the literature and to contribute to future research which correlate physical properties with new structural distortions.

2. Experimental

2.1. Sample preparation and selection of crystals

Pure and doped LiNH$_4$SO$_4$ (LAS) crystals, with different concentrations of Er^{3+}, Yb^{3+} and Dy^{3+}, were grown at 298, 308 and 313 K from aqueous solutions by slow evaporation (see Table 1). Pure LAS was obtained at equimolar quantities of Li$_2$SO$_4$ and (NH$_4$)$_2$SO$_4$; whereas for the doped compounds, the molar ratio was 1:1:*x*, where *x* is the concentration of the corresponding rare earth sulfate [RE$_2$(SO$_4$)$_3$]. All reagents had a purity grade of 99.99%. At least four syntheses were performed for each temperature and concentration, for all compounds studied.

Although α-LAS usually crystallizes below 293 K and β-LAS grows above this temperature (Mel'nikova *et al.*, 2003), by visual and microscopic analysis, a marked difference was observed in the crystalline habits of obtained single crystals under our conditions. According to Mel'nikova *et al.* (2003) and Mata-Ramírez (2002), the samples with polyhedral and cylindrical shapes were classified as β-habit (see Figs. 1*a* and *b*). While the very thin (millimetric thickness), flat and transparent layers, with rectangular or square shapes, of the samples were classified as α-habit (Fig. 1*c*). After the classi-fication of the crystals obtained from experiments, they were counted and divided into two parts: one for the analysis of single crystals and the other one to grind for the analysis of polycrystalline samples.
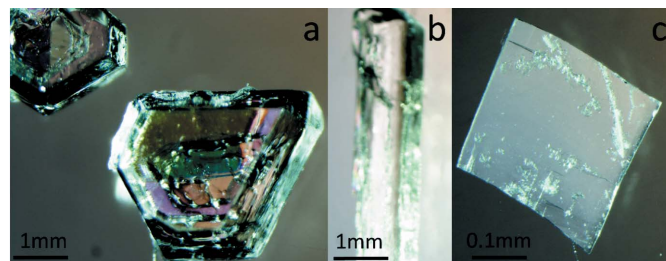
Figure 1
Samples of LiNH$_4$SO$_4$ with different crystalline habits: (*a*), (*b*) β-habit, and (*c*) α-habit for doped with Yb^{3+} crystal.

Table 2
Single crystal and refinement data for the α_1-LAS and α_2-LAS polytypes.

Identification code	α_1-LAS Yb 2 mol%	α_2-LAS Yb 4 mol%
Crystal data		
Empirical formula	$H_{3.940}LiN_{0.984}O_4SYb_{0.005}$	$H_{3.843}LiN_{0.961}O_4SYb_{0.013}$
M_r	121.54	122.51
Crystal system, space group	Monoclinic, $P2_1/c$	Monoclinic, $P2_1/c$
Temperature (K)	293	293
Wavelength (Å)	0.71073	0.71073
a, b, c (Å)	17.856 (8), 5.008 (3), 10.264 (13)	10.177 (15), 5.106 (4), 34.234 (16)
β (°)	106.46 (5)	90.20 (10)
V (Å^3)	880.2 (13)	1779 (3)
Z	8	16
$F(000)$	497	1000.0
D_x (Mg m^{-3})	1.836	1.831
Radiation type	Mo $K\alpha$	Mo $K\alpha$
μ (mm^{-1})	0.73	0.89
Crystal size (mm^3)	$0.18 \times 0.14 \times 0.09$	$0.17 \times 0.11 \times 0.09$
Data collection		
Diffractometer	Enraf–Nonius CAD4	Enraf–Nonius CAD4
Absorption correction	–	–
No. of measured, independent and observed [$I > 2\sigma(I)$] reflections	4811, 2549, 2020	9573, 5071, 3231
R_{int}	0.0905	0.068
$(\sin \theta/\lambda)_{max}$ (Å^{-1})	0.705	0.704
Range of h, k, l	$h = -25 \rightarrow 0, k = -7 \rightarrow 7, l = -13 \rightarrow 14$	$h = -14 \rightarrow 14, k = -7 \rightarrow 7, l = -48 \rightarrow 0$
Completeness to θ (%)	99.90 ($\theta = 25.242°$)	100 ($\theta = 25.242°$)
Refinement		
Refinement method	Full-matrix least-squares on F^2	Full-matrix least-squares on F^2
Final R indices [$I > 2\sigma(I)$]	$R_1 = 0.0535, wR_2 = 0.1354$	$R_1 = 0.0603, wR_2 = 0.1333$
R indices (all data)	$R_1 = 0.0671, wR_2 = 0.1434$	$R_1 = 0.1029, wR_2 = 0.1632$
Goodness-of-fit on F^2	1.173	1.197
No. of reflections, restraints, parameters	2549, 74, 153	5071, 0, 256
$\Delta\rho_{max}, \Delta\rho_{min}$ (e Å^{-3})	1.05, −0.68	1.89, −1.04

2.2. Thermal analysis

Differential scanning calorimeter (DSC) analysis was performed in order to study the stability of all selected, doped and pure, single crystals with different habits. DSC measurements were carried out on a Perkin–Elmer differential scanning calorimeter Pyris I-DSC, under nitrogen gas in a sequential cycle: $298 \rightarrow 190 \rightarrow 575 \rightarrow 190$ K, using a heating and cooling rate of 10 K min^{-1}.

2.3. X-ray diffraction

XRD data were obtained by using three different experimental protocols. Two of them related to single crystals and the third one for powder samples.

(i) Two single crystals of Yb-doped LAS with 2 and 4 mol% (nominal concentrations), and α-habit were selected. Diffraction data at 293 K were collected on a MARS345 automated diffractometer, with an image-plate detector and using monochromatic Mo $K\alpha$ radiation by reflection from a graphite crystal. The structures were solved by Patterson's method, using *SHELXS* (Sheldrick, 2015), and refined by full-matrix least-squares using *SHELXL* (Sheldrick, 2015). For

details of the data collection and the structure determination see Table 2 and the CIF files in the supporting information.

(ii) On the other hand, single crystals with an α-habit were measured with the Agilent SuperNova diffractometer, in order to study the thermal dependence of their reciprocal space images and lattice parameters at low temperatures (from 200 to 295 K). The *CrysAlisPro* computer software (Agilent, 2014) was used during the data analysis and also for diffractometer control and data collection.

(iii) Powder diffraction measurements were performed for all doped and pure LAS samples, using a PANalytical X'Pert Pro diffractometer (Bragg–Brentano mode) equipped with an X'Celerator detector using Cu $K\alpha_1$ radiation. The angular range $5 > 2\theta > 100°$ was scanned at a step size of 0.02° and 200 s step time. Divergence and anti-scatter slits were set at 1 and 0.5°, respectively, and the detector was used in a scanning mode with an active length of 2.14°. A 0.02 rad Soller slit was used in the diffraction beam. Measurements at different temperatures were carried out during a cyclic process of heating and cooling: $298 \rightarrow 548 \rightarrow 298$ K using an Anton Paar HTK–2000 chamber and under air atmosphere. The heating and cooling rate was 10 K min^{-1} and the sample kept at the selected temperature for 5 min to stabilize before the scan. Whole pattern fits were performed using the *FullProf* computer program (Rodríguez-Carvajal, 1993). In addition, to compare the obtained crystal structures, we performed a symmetry-mode analysis of the more distorted structure with respect to the more symmetric one, by using the *AMPLIMODES* program (Orobengoa *et al.*, 2009), available on the Bilbao Crystallographic Server (Aroyo *et al.*, 2011).

2.4. Dielectric spectroscopy

Dielectric measurements (real ε'_r and imaginary ε''_r parts of complex permittivity) were performed on single crystals, using an HP 4192A impedance analyzer in the frequency range from 0.1 kHz to 1 MHz with an AC signal amplitude of 1 V. Three single crystals were selected: one β-LAS with cylindrical shape (height 2.0 mm and diameter 3.0 mm) was cut with the c-axis (pseudo-hexagonal axis) parallel to the axis of the cylinder, and two single crystals with thin plate shapes: one pure α-LAS (obtained at room temperature), and one doped α-LAS Yb 1.4 mol%. After, the plane parallel faces for all crystal samples

Table 3
Atomic coordinates, equivalent isotropic displacement parameters and occupation factors for the α_1-LAS polytype.

U_{eq} is defined as one third of the trace of the orthogonalized U^{ij} tensor.

Atom	x	y	z	U_{eq} (10^{-3} Å^2)	Occ. factor
S1	0.4019 (1)	0.7881 (1)	0.3501 (1)	16 (1)	1.0
O11	0.4075 (1)	0.7062 (5)	0.4897 (2)	28 (1)	1.0
O12	0.4109 (1)	1.0821 (4)	0.3465 (2)	31 (1)	1.0
O13	0.3261 (1)	0.7155 (5)	0.2583 (2)	36 (1)	1.0
O14	0.4649 (1)	0.6618 (4)	0.3038 (2)	24 (1)	1.0
S2	0.0981 (1)	0.2884 (1)	0.4473 (1)	15 (1)	1.0
O21	0.0925 (1)	0.2049 (5)	0.5819 (2)	26 (1)	1.0
O22	0.0894 (1)	0.5822 (4)	0.4341 (2)	29 (1)	1.0
O23	0.0049 (1)	0.1605 (4)	0.3389 (2)	22 (1)	1.0
O24	0.1740 (1)	0.2124 (5)	0.4303 (2)	34 (1)	1.0
Yb1	0.3329 (1)	0.2738 (5)	0.0677 (2)	31 (1)	0.0051 (12)
N1	0.3329 (1)	0.2738 (5)	0.0677 (2)	31 (1)	0.985 (4)
Yb2	0.1673 (1)	0.7751 (5)	0.2335 (3)	31 (1)	0.0054 (12)
N2	0.1673 (1)	0.7751 (5)	0.2335 (3)	31 (1)	0.984 (4)
Li1	0.0011 (2)	0.2967 (9)	0.1505 (4)	20 (1)	1.0
Li2	0.5016 (2)	0.2965 (10)	0.3519 (5)	23 (1)	1.0
H11	0.277 (1)	0.290 (6)	0.031 (3)	47	0.985 (4)
H12	0.351 (2)	0.137 (5)	0.016 (3)	47	0.985 (4)
H13	0.357 (2)	0.439 (3)	0.055 (3)	47	0.985 (4)
H14	0.346 (2)	0.224 (6)	0.161 (1)	47	0.985 (4)
H21	0.223 (1)	0.773 (6)	0.255 (3)	46	0.984 (4)
H22	0.145 (2)	0.660 (5)	0.157 (2)	46	0.984 (4)
H23	0.151 (2)	0.713 (6)	0.310 (2)	46	0.984 (4)
H24	0.148 (2)	0.953 (3)	0.209 (3)	46	0.984 (4)

were coated with silver paste and then placed into the cell (parallel plate capacitor). The measurements were recorded in two different runs: (1) heating from 190 until 290 K, using a homemade cryostat, and (2) above room temperature, following the cycle: $298 \rightarrow 520 \rightarrow 298$ K using a resistance furnace, with a warming and cooling rate of 0.8 K min^{-1}. In both experiments, the temperature was monitored using a thermocouple within an accuracy of approximately 0.1 K. In order to gain a deeper knowledge of the dielectric behavior, we performed a conductivity spectra analysis. It is based on the Universal Dielectric Response (UDR; Jonscher (1977; Ngai et al., 1979; Dissado & Hill, 1979). According to this model, the real part of the conductivity spectra σ' tends towards the DC conductivity (σ_{dc}) as the frequency (ν) decreases and shows a dispersive regime where the conductivity strongly increases with the frequency. A slightly different version of the more typical Jonscher equation is given by León et al. (1997)

$$\sigma'(\nu) = \sigma_{dc}\left[1 + \cos\left(\frac{s\pi}{2}\right)\left(\frac{\nu}{\nu_p}\right)^s\right], \qquad (1)$$

where s is a fractional exponent with values between 0 and 1, depending on the many-body interactions among charge carriers, and ν_p is crossover frequency.

3. Results and discussion

3.1. Effect of the doping in the LAS single crystals

Taking into account the crystals identified as α- and β-habits, obtained from each experiment, we found for pure

compounds at 298, 308 and 313 K only 5% of an α-habit. However, by doping the compounds with rare earth ions (Er^{3+} and Yb^{3+}), at the same evaporation temperatures, it was possible to obtain a bigger proportion of crystals with the α-habit; reaching a percentage of 15%. The crystals with better quality were obtained for concentrations of Er^{3+} ions between 0.6 and 1.2 mol% and for concentrations of Yb^{3+} ions from 0.7 mol% thereafter. In the cases where we used Dy^{3+} as a dopant, with the concentrations given in Table 1, we did not obtain the α-habit. Therefore, as a first result, when we doped the samples with the Er^{3+} and Yb^{3+} ions above and at room temperature the α-habit is favored.

In order to evaluate the thermal stability of the doped LAS crystals, we have compared the DSC curves of single crystals with both α- and β-habits. The results obtained for pure β-LAS crystals (Fig. 2a) are comparable to those found in the literature (Połomska, 2001; Połomska et al., 1994). The curve shows two characteristic peaks: the ferroelastic–ferroelectric phase transition at 287 K and the ferroelectric–paraelectric one at 461 K.

In the case of the α-LAS Yb 0.7 mol% (nominal value; Fig. 2b), the phase transition at low temperature seems precluded. At high temperature, the ferroelectric–paraelectric transition takes place at 484 K and it is accompanied by a post-transition around 500 K. This more complex transition adds an enthalpy change almost one order of magnitude greater than the ferroelectric–paraelectric transition observed for β-LAS. However, in the case of α-LAS Yb 0.7 mol%, as the temperature decreases, the paraelectric–ferroelectric transition was recovered, although the low-temperature transition was not well distinguished. In this process, the crystal recovered the β-habit. Very similar behavior was observed in other single crystals with α-LAS habit. Thermal analysis has revealed that the $\alpha \rightarrow \beta$ transition takes place at high temperature and it must be the reconstructive and irreversible transition observed by Komornicka et al. (2014).
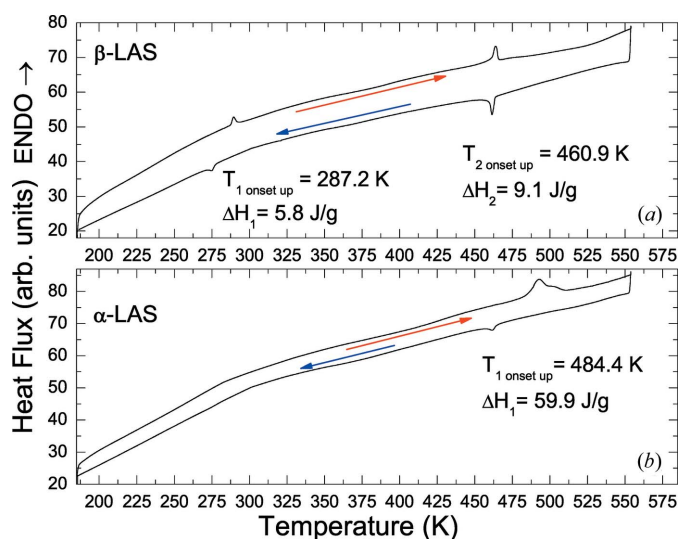
Figure 2
DSC curves correspond to single crystals: (a) for the pure compound with the β-habit (reference sample) and (b) for the α-LAS Yb^{3+} 0.7 mol%.

Table 4
Atomic coordinates, equivalent isotropic displacement parameters and occupation factors for the α_2-LAS polytype.

U_{eq} is defined as one third of the trace of the orthogonalized U^{ij} tensor.

Atom	x	y	z	U_{eq} (10^{-3} Å^2)	Occ. factor
S1	0.6481 (1)	0.7331 (1)	0.2009 (1)	6 (1)	1.0
O11	0.6399 (4)	0.4374 (5)	0.2061 (1)	41 (1)	1.0
O12	0.7859 (3)	0.8058 (10)	0.2041 (1)	52 (1)	1.0
O13	0.5709 (3)	0.8568 (6)	0.2324 (1)	27 (1)	1.0
O14	0.5950 (4)	0.7924 (10)	0.1631 (1)	57 (1)	1.0
S2	0.8982 (1)	0.2837 (2)	0.0492 (1)	17 (1)	1.0
O21	0.8934 (3)	0.5828 (6)	0.0441 (1)	32 (1)	1.0
O22	1.0370 (3)	0.2110 (6)	0.0462 (1)	30 (1)	1.0
O23	0.8456 (3)	0.2180 (7)	0.0867 (1)	37 (1)	1.0
O24	0.8213 (3)	0.1630 (6)	0.0180 (1)	28 (1)	1.0
S3	0.3996 (1)	0.2162 (2)	0.0490 (1)	17 (1)	1.0
O31	0.5355 (3)	0.2891 (6)	0.0463 (1)	30 (1)	1.0
O32	0.3211 (3)	0.3371 (6)	0.0174 (1)	27 (1)	1.0
O33	0.3916 (3)	−0.0811 (6)	0.0447 (1)	33 (1)	1.0
O34	0.3434 (3)	0.2813 (7)	0.0875 (1)	32 (1)	1.0
S4	0.1488 (1)	0.8032 (3)	0.2009 (1)	36 (1)	1.0
O41	0.1414 (3)	1.1054 (7)	0.2046 (1)	31 (1)	1.0
O42	0.2864 (2)	0.7278 (5)	0.2036 (1)	21 (1)	1.0
O43	0.0927 (3)	0.7312 (6)	0.1630 (1)	27 (1)	1.0
O44	0.0714 (3)	0.6850 (7)	0.2325 (1)	29 (1)	1.0
N1	0.4006 (3)	0.2369 (6)	0.1662 (1)	42 (1)	0.907 (4)
N2	0.6508 (3)	0.7697 (7)	0.0838 (1)	36 (1)	0.959 (4)
N3	0.1517 (3)	0.7309 (7)	0.0833 (1)	33 (1)	0.978 (4)
N4	0.9005 (4)	0.2744 (9)	0.1667 (1)	38 (1)	1.0
Yb1	0.4006 (3)	0.2369 (6)	0.1662 (1)	42 (1)	0.0311 (15)
Yb2	0.6508 (3)	0.7697 (7)	0.0838 (1)	36 (1)	0.0137 (15)
Yb3	0.1517 (3)	0.7309 (7)	0.0833 (1)	33 (1)	0.0074 (14)
Li1	0.3992 (7)	0.7198 (14)	0.2497 (2)	24 (1)	1.0
Li2	0.1017 (7)	0.3041 (15)	0.2508 (2)	28 (2)	1.0
Li3	0.1488 (7)	0.2123 (13)	0.0001 (2)	22 (1)	1.0
Li4	0.6491 (6)	0.2976 (12)	0.0013 (2)	19 (1)	1.0

3.2. Structural characterization of two new polytypes

Two different polytypes, with an α-habit, were solved in the same space group $P2_1/c$ for ytterbium-doped LAS crystals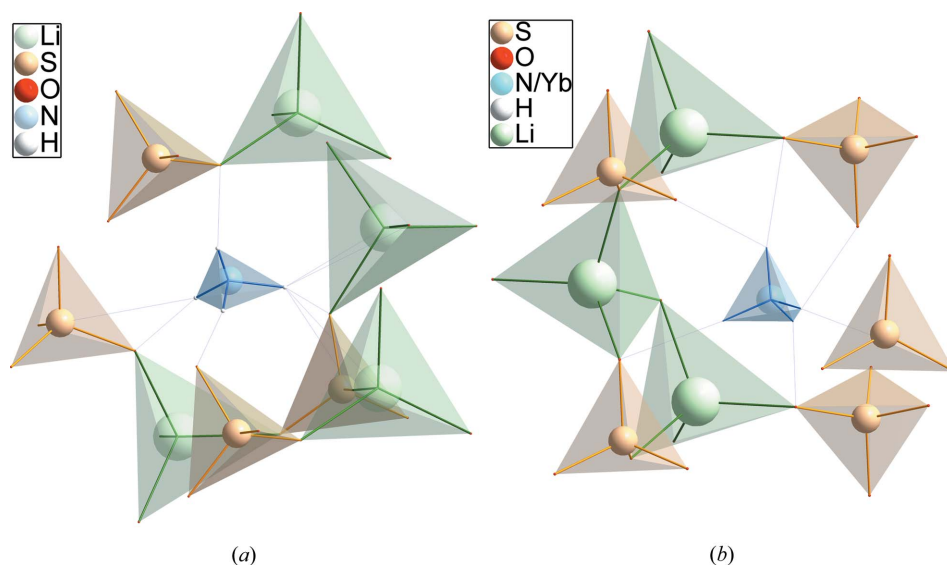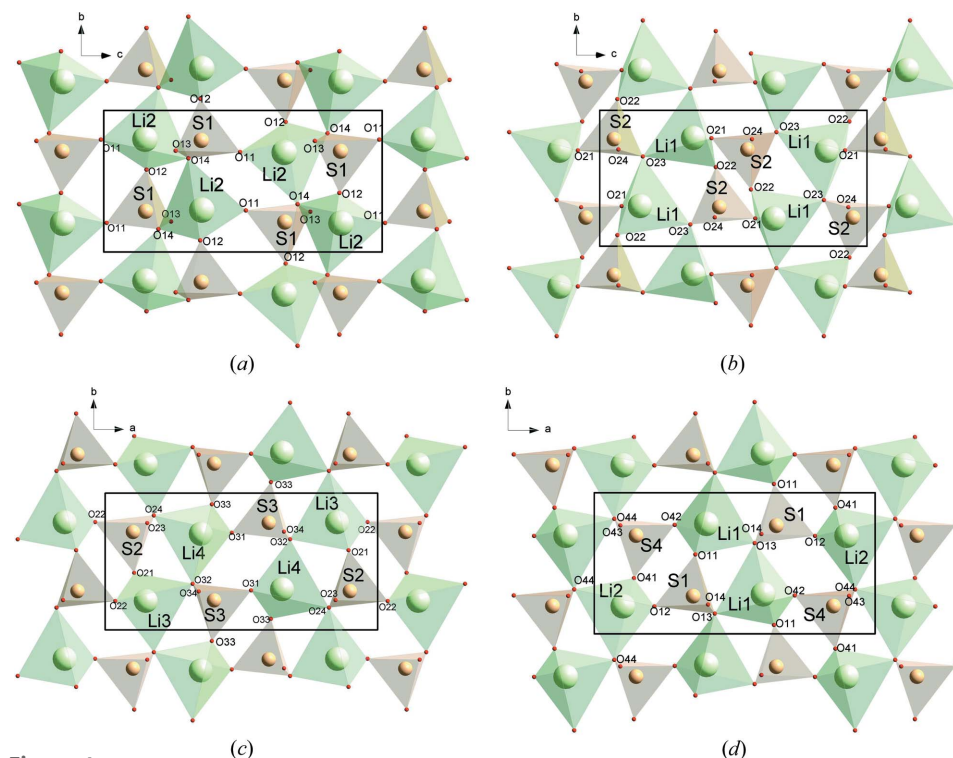 with 2 and 4 mol% (nominal concentrations) and these phases were named α_1- and α_2-LAS, respectively (see Table 2). The atomic coordinates, equivalent thermal displacement and occupation factor are shown in Tables 3 and 4; including the atomic coordinates of the H atoms, which were calculated only for α_1-LAS. The bond lengths as well as the angles are given as CIF files attached as supporting information. The refinement of the ammonium sites indicates that NH_4^+ and Yb^{3+} are located at the same position, in agreement with the electron density residuals found in the difference Fourier maps (see Table 2). Note that the substitution of ammonium by ytterbium is not homogeneous and the experimental concentrations, calculated from the occupation factors, are 0.5 and 1.3 mol% for the α_1-LAS, and the α_2-LAS, respectively. These values are less than the nominal concentrations: 2 and 4 mol%.

In general, we have observed that the α-habit was favored by doping with ions of smaller ionic radii than the ammonium one; this can be explained from the obtained crystal structures. The ammonium sites in both polytypes, α_1- and α_2-LAS, lead to an environment with six first neighbors, which is a more typical geometry for heavy rare earth ions like Yb^{3+} and Er^{3+} (Guzmán-Afonso et al., 2011; Maczka et al., 2012). Moreover, although the ionic radius of Dy^{3+} is closer to the NH_4^+ ion, this rare earth ion leads to an environment with coordination over seven O atoms; then, the structure of the ferroelectric β-phase must be favored (see Fig. 3). For the α_1-LAS structure, the ammonium ion is surrounded by ten O atoms; six of them are closer to the ammonium cation (see Fig. 3b). For the ferroelectric β-phase, nine O atoms (Mata-Ramírez, 2002) surround the NH_4^+ cation; in this case, it is more difficult to distinguish a clear subgroup of first neighbors (see Fig. 3a). This fact can explain why we have not obtained doped α-LAS with dysprosium.

The S and Li atoms are at the center of oxygen tetrahedra which share corners in order to form the $[LiSO_4]^-$ layers perpendicular to the a axis in α_1-LAS, and to the c axis in α_2-LAS. The NH_4^+ ions are located between the layers. All the H atoms of the NH_4^+ group form hydrogen bonds with O atoms of the nearest layers. Both α-structures consist of the same stacked layers, with the following lattice parameter relationships: $a_2 = -c_1$, $b_2 = -b_1$, $c_2 = -2a_1 - c_1$ and with a translation vector (0 0 −1/2). The two different $[LiSO_4]^-$ layers for each compound are shown in Fig. 4. For α_1-LAS, these layers are parallel to the planes (h00) and there are only one sulfate and one lithium ion in the asymmetric unit of each layer (labeled 1–1 and 1–2). Then the O13 and O24 atoms do not belong to the lithium tetrahedra, while two O14 atoms and two O23 atoms are

Figure 3
Views of the two environments for the ammonium cation in ferroelectric (a) β-LAS and (b) α_1-LAS. The other environments for the ammonium cation in both polytypes: α_1- and α_2-LAS, are very similar.

connected to the Li2 and Li1 atoms, respectively, in each layer. This scheme of bonds leads sulfate tetrahedra with bonds from 1.456 (2) to 1.487 (2) Å and lithium tetrahedral coordination from 1.929 (5) to 1.976 (5) Å (see the CIF files in the

Figure 4
Comparison of layers for the polytypes: α_1-LAS (upper), called layers 1–1 (left) and 1–2 (right) and α_2-LAS (bottom), called layers 2–1 (left) and 2–2 (right). There are a number of differences between the non-symmetric layers and between both compounds.
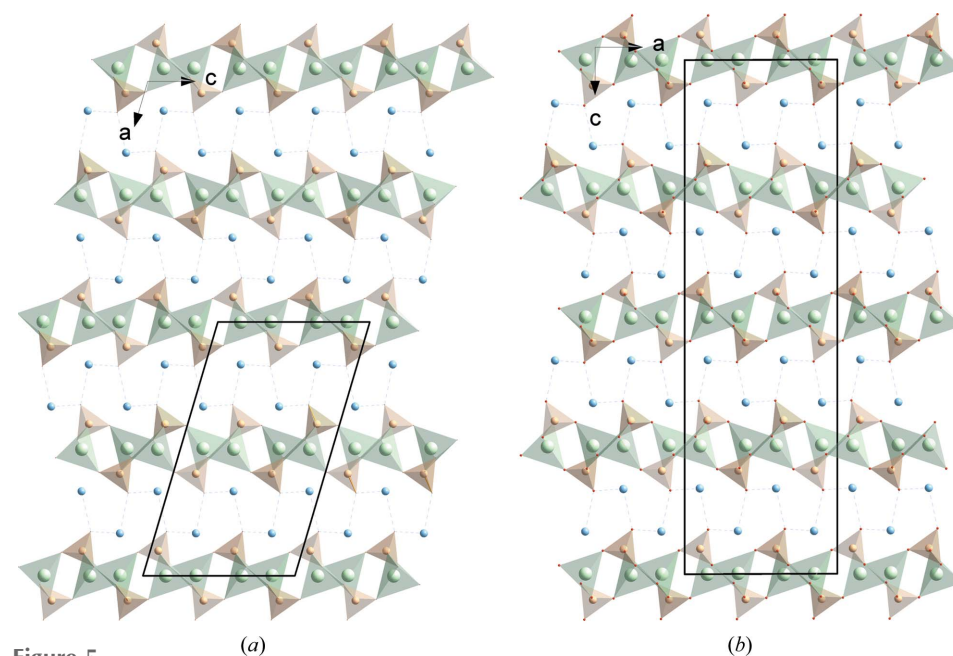
Figure 5
View of the layered structure. For (a) α_1-LAS, the layers 1–1 and 1–2 are at the top and the middle of the unit cell. For (b) α_2-LAS, the layers 2–1 and 2–2 are at the top and just below the unit cell. The other layers are generated by symmetry.

supporting information). For α_2-LAS, these layers are parallel to the (00l) planes and there are two sulfate ions and two lithium ions in the asymmetric unit of each plane (labeled 2–1 and 2–2). The O23 and O34 atoms are not connected to the Li3 and Li4 atoms in the 2–1 layer and the O14 and O43 atoms do not belong to the Li1 and Li2 tetrahedra in the 2–2 layer; here there are no symmetry-related atoms in any tetrahedral coordination of the Li atoms. Now, the scheme of the bonds is more distorted, with bonds from 1.434 (3) to 1.527 (3) Å for sulfate tetrahedra and from 1.890 (8) to 2.066 (8) Å for lithium tetrahedral coordination (see the CIF files in the supporting information). For the structure proposed by Komornicka *et al.* (2014) there are two tetrahedra of sulfur and two of lithium, which are not related by symmetry in a unique layer, and the O atoms are connected similarly to each layer in the α_2-LAS structure.

In Fig. 5, both stacking layers are shown, where the ammonium ions connect two consecutive layers. Here, only the N atoms from the ammonium ions are plotted. Note that for α_2-LAS, the periodicity along the direction [00l] is doubled with respect to the corresponding one for α_1-LAS. This is due to the translation of $c/2$ given by symmetry requirements (a glide plane perpendicular to the b axis).

In order to quantitatively compare both polytypes: α_1- and α_2-LAS, we have calculated the total distortion between them by using the *AMPLIMODES* computer program (Orobengoa *et al.*, 2009). The distortion of α_2-LAS, with respect to α_1-LAS, can be decomposed into two symmetry modes, given by the irreducible representations *GM1+* (at the center of the Brillouin zone) and *Y2+* [at the point $\Delta(1/2, 0, 0)$ of the Brillouin zone]. The amplitude of the second mode is close to 2 Å longer than the first one (5.226 and 3.338 Å, respectively). This indicates that the crystal structure of α_2-LAS cannot be well described with the crystal structure of α_1-LAS. In general, the O-atom

displacements are larger than those of the S, Li and N atoms and their contributions to the distortion are more important.

The obtained layered structures are consistent with other α-LAS polytypes and $LiNH_4SeO_4$ (LASe) found in the literature (Pietraszko & Lukaszewicz, 1992; Waśkowska & Allmann, 1982; Tomaszewski, 1992a) which were described in the orthorhombic space group $Pbn2_1$. Very recently, Komornicka et al. (2014) modeled possible structures for $LiNH_4SO_4$ leading the formation of different polytypes. They combine a different sequence of layers of A and B types, where each layer is composed of stripes (S+/S-) oriented in ferroelectric or antiferroelectric (AF) order. In particular, they determined a crystal structure in the space group $Pca2_1$ with $a = 10.195$ (2), $b = 4.9967$ (10) and $c = 17.127$ (3) Å, with layers containing AF domains. The A and B stacked layers are symmetrically related. None of our two structures are completely described with the proposed model, as we can see in Figs. 4 and 5. The α_1-LAS polytype has two different layers in the unit cell (layers 1–1 and 1–2) that are not related by symmetry. However, the domains of AF type, in each layer, are related by symmetry. The unit cell for the α_2-LAS polytype is formed by four layers related by symmetry in pairs (from the layers 2–1 and 2–2), but the domains of each layer are AF type and are not related by symmetry.

Lima et al. (2003) have characterized new crystals of the lithium sulfate family: the caesium lithium sulfate, $Cs_{1.15}Li_{2.85}(SO_4)_2$, and the caesium lithium rubidium sulfate, $Cs_{0.90}Li_{2.88}Rb_{0.22}(SO_4)_2$. These compounds are described and discussed in the context of the simple and double polymorphism. Authors associated the typical pseudo-hexagonal axes of double sulfates in the β-ferroelectric phase with the orthorhombic (or monoclinic) cells in the α-modification, where one of the axes of the α-modification corresponds, approximately, to that measured in double sulfates of the β-phase, but where the other axis is shorter. They explained this contraction was due to the low occupation of the heavy-ion sites (in this case, Rb and Cs), which was responsible for the new framework. Both, α and β, polymorphs are again compared in Fig. 6. The β-phases are clearly denser than the α-polytypes. The connectivity between structural groups is also different: the β-phases are built connecting all the vertices of the SO_4 and LiO_4 tetrahedra in a three-dimensional structure, while the α-phases are arranged as the layered structure described above. Moreover, we can see the same chains of combined SO_4 and LiO_4 tetrahedra placed parallel to the a and c axis, respectively. Note that the vertices are connected in two different ways: for the ferroelectric β-phase, the two connected chains are related by a glide plane (the plane of the figure) with a translation, which is parallel to the axes of both chains. For the α_2-phase, the two connected chains are related by a 2_1 screw axis, parallel to the b axis, and followed by a translation of $c/2$. Therefore, we have found a structural motif that leads to both polymorphs having a common crystallographic axis with the same (or multiple) length. Now we can explain some of the controversies between these two structural types: on one hand, similar space groups, and on the other, a common lattice parameter. As an example, the structure reported in the ICSD database (Belsky et al., 2002) for the NH_4LiSeO_4 is misclassified since it has been considered like the β-type (probably because both have the same space group). Furthermore, it would allow the coexistence of phases belonging to the α- and β-phases, due to an intergrowth from the common axis.

3.3. Structural stability of α-LAS

A deeper analysis was performed for doped ground crystals of the α-LAS habit with Yb 1.4 mol%, Yb 0.7 mol% and Er 0.6 mol% (nominal concentration), which were measured using XRD in the temperature cycle of $298 \rightarrow 548 \rightarrow 298$ K.

Fig. 7 shows the diffractograms of a complete cycle for doped LAS Er^{3+} 0.6 mol% (nominal concentration) and the profile matching, where the well known ferroelectric β-LAS phase and any α-LAS polytypes are present. The presence of, at least, these two polymorphs can be visualized by the Bragg reflections. It was impossible to distinguish between α_1- and α_2-LAS structures. Both phases and other new different α-polytypes can coexist in the powder sample. We used α_1-LAS cell parameters to perform the refinements of peaks which did not belong to the ferroelectric β-LAS phase. Thus, we cannot strictly say that the α_1-LAS polytype was found for samples doped with Er^{3+}.

The results of the refinements provided the reliability factors: χ^2, R_B and R_{wp}, which varied from 1.5 to 2.4, from 0.7 to 1.8% and from 0.3 to 2.3%, respectively. Thermal dependence of the lattice parameters between 200 and 548 K are presented in Fig. 8 as well as the concentration of the mixture of α and β polytypes, which was calculated from the intensity of their two characteristic peaks at low angles (around ~ 10.5 and $\sim 13.5°$), given the theoretical intensities. On heating, the α-LAS Er 0.6 mol% polytype coexists ($\sim 38\%$) with the
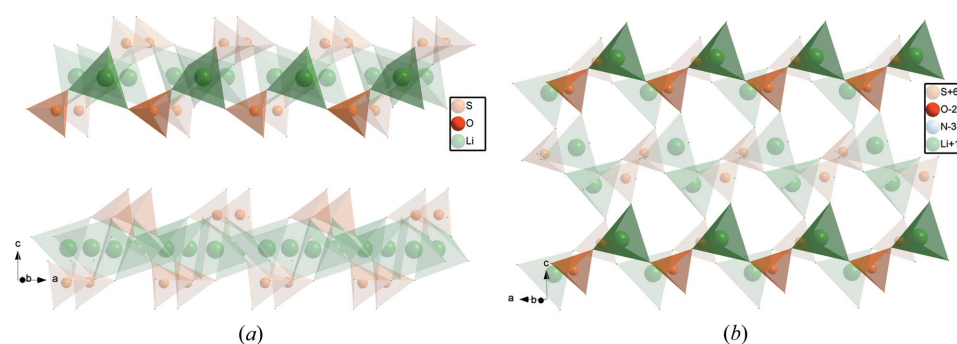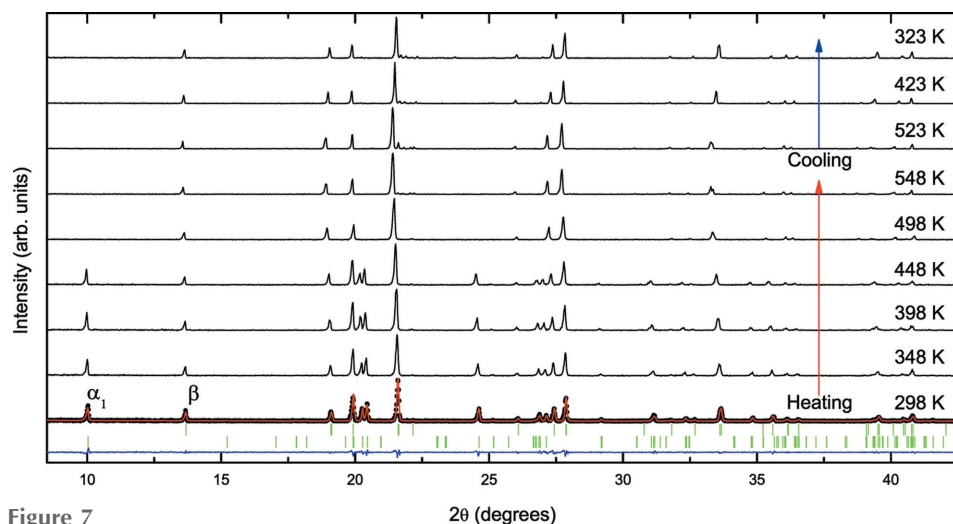

Figure 6
View of the structures of (a) the α_2-polytype and (b) the ferroelectric β-phase, showing different typologies. Chains of SO_4 and LiO_4 tetrahedra connected in different ways to form each structural type: α and β. Note that there is an axis with the same length or multiples thereof in both structures.

Figure 7
Diffractograms of LAS Er 0.6 mol% powder samples measured on heating and cooling. Observed data are shown in black. As an example, at the bottom of the figure, the profile fit is shown by red lines and the difference between the observed and calculated profiles is plotted by blue lines. The green vertical bars represent the Bragg reflections. The upper group of reflections belongs to ferroelectric β-LAS and the lower ones to α-LAS Er 0.6 mol%. Two marked peaks are used for faster identification.

We did not perform low-temperature XRD measurements in polycrystalline samples because ytterbium(III) in doped samples can be reduced to ytterbium(II), during the cooling process, by using an Anton Paar TTK camera under vacuum. We observed changes in the diffractogram at lower temperatures but we did not investigate it. Therefore, diffraction data were measured for single crystals (doped LAS–Er 1.2 mol% and LAS–Yb 1.4 mol%, nominal values) with the α-habit, at different temperatures: 200, 240, 250, 260, 273 and 295 K. Reciprocal space images showed the existence of weak and diffuse reflections along c^*, as described by Komornicka *et al.* (2014). Thus, diffraction data were not suitable to solve its crystal structure. However, we were interested in determining the thermal dependence of the lattice parameters. We refined the lattice parameters of α_1-LAS as an average structure of the α-modification. In the low-temperature range, the structure remains unchanged, *i.e.* we did not observe any phase transition, in particular at 250 K, as suggested in the literature (Połomska *et al.*, 1994; Mel'nikova *et al.*, 2003) nor at 283 K, where the ferroelastic–ferroelectric transition occurs. However, we observed a very slight anomaly in the thermal dependence of the a and c lattice parameters and the β angle, between 240 and 260 K (see Fig. 8, for the sample α-LAS Yb 1.4 mol%). The observed anomaly could be due to the coexistence of the α- and β-polymorphs, even for single crystals as it was shown for polycrystalline samples. As we have shown in the previous section, an intergrowth between different α- and β-polymorphs belonging to both phases is quite possible.

ferroelectric β-LAS until 448 K (see Figs. 7 and 8). Above this temperature, the first characteristic peak disappears. This result was also found by Komornicka *et al.* (2014). Note that at 460 K the ferroelectric β-phase undergoes a transition to the paraelectric one. Then, at 484 K (from DSC) or 498 K (from XRD), from our data, the phase β-LAS must be paraelectric. In Fig. 8, the thermal dependence of the lattice parameters confirms, definitively, the α-LAS to paraelectric β-LAS phase transition. Moreover, the XRD cooling cycle, just like the previous DSC, reveals the irreversibility of the process; as it was expected.

3.4. Comparative dielectric analysis of pure and doped LAS

In this section, we have performed a detailed study of the dielectric properties for doped and pure LAS single crystals with α-habit for the first time, in order to complete and confirm the results obtained by XRD and thermal analysis, at the same range of temperatures. A single crystal with β-habit was used as a reference material.
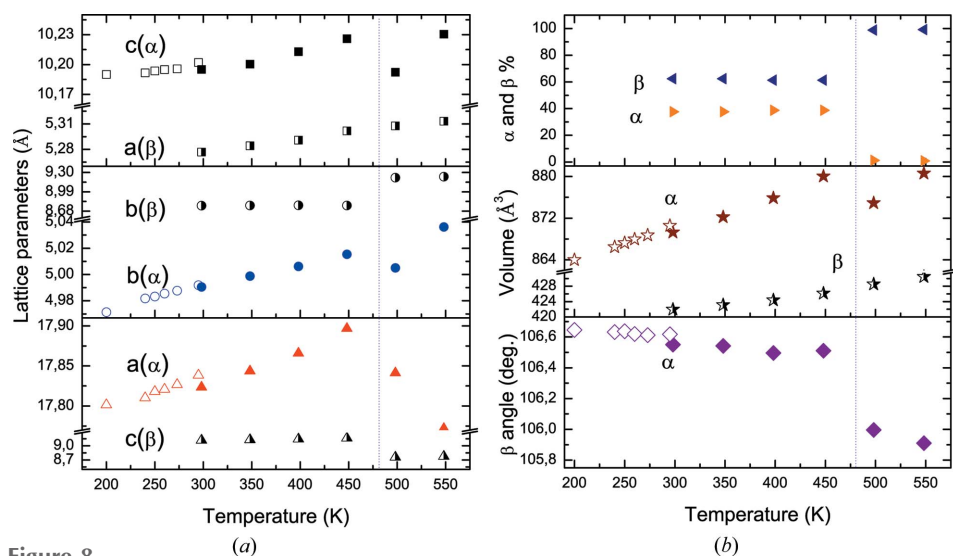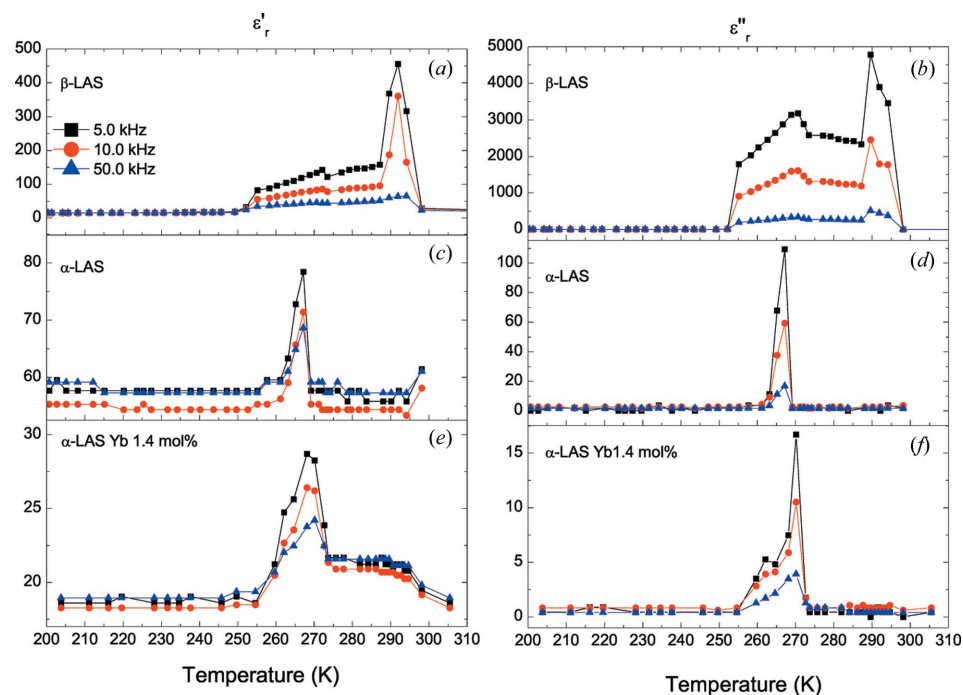

Figure 8
Thermal dependence of the lattice parameters a, b, c, β angle, volume and concentration percent of α-LAS Yb 1.4 mol%. Data collected by single-crystal XRD, between 200 and 298 K, are indicated with empty symbols. Data collected by XRD in polycrystalline samples, between 298 and 548 K, are indicated with full symbols for α-phases and with half-full symbols for β-phases. The vertical dashed line indicates the ferro-paraelectric phase transition.
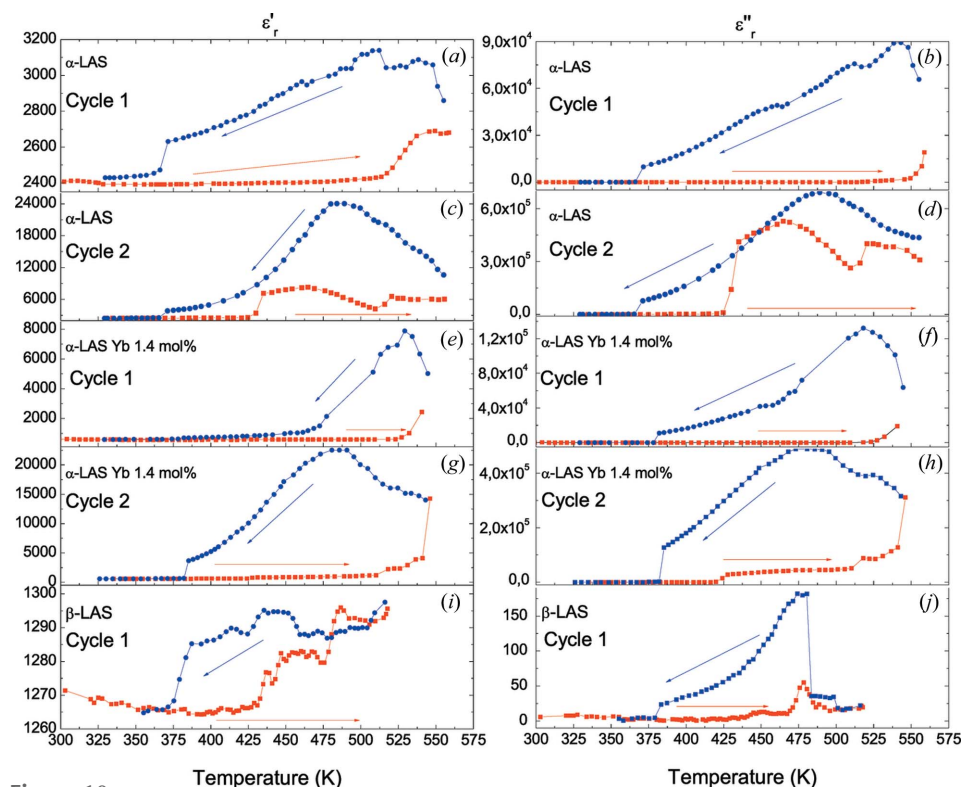
Below room temperature, the β-LAS crystal shows an abrupt change in ε_r' and ε_r'', which takes place close to 290 K, with a pre-transition around 250 K (Figs. 9a and b). Other authors also comment on the existence of a pre-transition, especially Gaffar & El-Fadl (1999) and Połomska (2001). It was attributed to the existence of an order–disorder process that extends over a long range of temperatures. This temperature corresponds to the well-known ferroelastic–ferroelectric phase transition. The single crystals with the α-habit (pure α-LAS and α-LAS Yb 1.4 mol%) show a peak in ε_r' and ε_r'' at 273 K (see Figs. 9c–f). However, unlike Komornicka et al. (2014), we did not consider any phase transtion because the crystal structure remains with the space group $P2_1/c$ and without changes in the crystal habit, in this range of temperatures. Then this anomaly in the dielectric properties can be due to the mentioned residual inter-growth between both poly-morphous. Note that the temperature of this jump is close to the ferroelastic–ferroelectric phase transition. We have already observed slight anomalies in the thermal dependence of the lattice parameters and the DSC curves, in this range of temperatures. More-over, the values of ε_r' and ε_r'', asso-ciated with this peak for α-LAS Yb 1.4 mol% and pure α-LAS, are much smaller than the corre-sponding values for β-LAS.

Fig. 10 shows the temperature dependence of ε_r' and ε_r'', at 10 kHz, during two heating–cooling cycles, for the pure α-LAS and α-LAS Yb 1.4 mol% single crystals. In the heating curves of the first cycle, any phase transition is observed until around 500 K, for both samples (Figs. 10a, b and e, f). It confirms that the α-phase is stable in the temperature range 298–500 K; also, it has been observed using DSC (Fig. 2) and XRD on polycrystal-line samples (Fig. 5). The dielectric anomaly observed around 500 K indicates the beginning of the $\alpha \rightarrow \beta$ phase transformation. We did not increase the temperature above 550 K because the decomposition of LAS is expected around this temperature. It is then possible the $\alpha \rightarrow \beta$ phase transition was incomplete. In the heating curves of
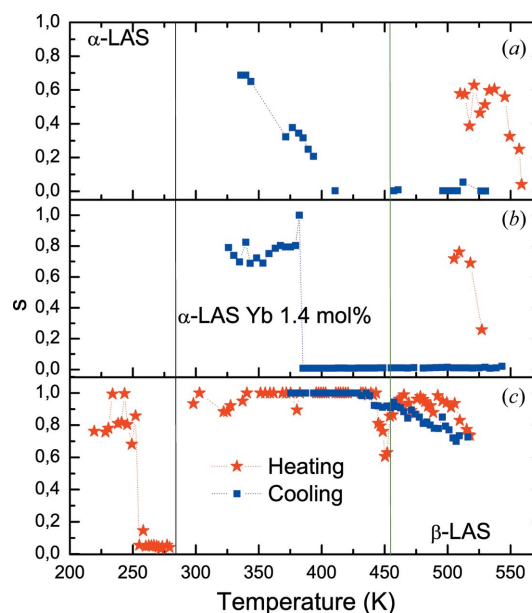

Figure 9
Variation of ε_r' and ε_r'' with temperature at 5, 10 and 50 kHz, collected between 220 and 300 K, for (a), (b) β-LAS, (c), (d) α-LAS and (e), (f) α-LAS Yb 1.4 mol%.

Figure 10
Variation of ε_r' and ε_r'' with temperature at 10 kHz, during two heating–cooling cycles (295 $\rightarrow$ 550 $\rightarrow$ 298 K) for (a), (b), (c), (d) α-LAS, (e), (f), (g), (h) α-LAS Yb 1.4 mol% and (i), (j) β-LAS crystals.

the second cycle (Figs. 10c, d and g, h), a similar behavior to that performed by the β-LAS crystal (reference sample, in Figs. 10i, j) can be seen, although it is much smoother. This dielectric behavior corresponds to the new β-phases transformed from pure α-LAS and α-LAS Yb 1.4 mol% ones, respectively. It is important to note that the reorder process occurs, in the first cooling (cycle 1), until 382 K, where a possible new phase transition is observed. Solans et al. (1999) found for the β-LAS a transformation, from the crystal structure at 318 K to the structure at 383 K, which consists of a rotation by 41° of the sulfate ions around an S—O bond. This may be the reason for the decrease of almost two orders of magnitude in the electrical conductivity between both temperatures. Thus, this result cannot be explained by a mixture of different components (α- and β-phases) as Tomaszewski (2000) suggests; at this stage, α-LAS polymorphs are precluded. At the end of the thermal experiment, all the samples: pure α-LAS and doped α-LAS with Er 0.6 mol%, Yb 0.7 mol% and Yb 1.4 mol% showed similar behavior and they were twinned crystals with the β-habit.

In Fig. 11 we show the frequency dependence of σ' at different temperatures, on heating (cycle 1) for both α- and β-habits. These curves have been adjusted to equation (1). It is important to note that the experimental values of σ' for the α-LAS polymorphs are very low between 200 and 496 K. Thus, only a few curves could be fitted to obtain the temperature dependence of σ_{dc}, ν_p and s using equation (1). Above 500 K the increasing conductivity allowed us to fit all these parameters.
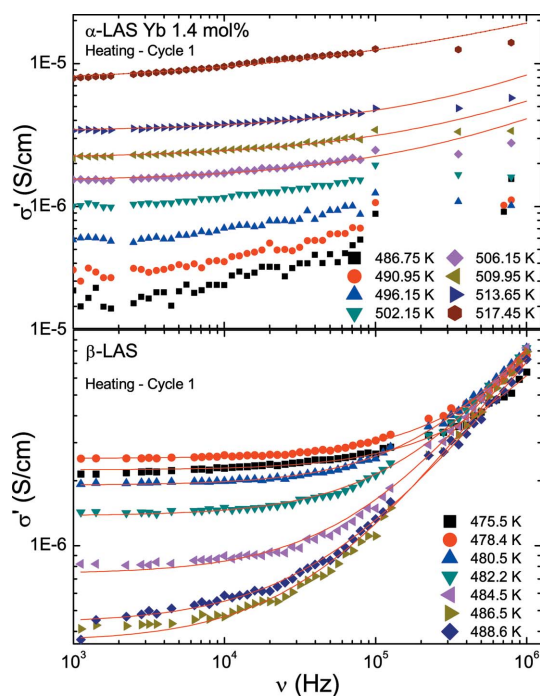
The s parameter, from equation (1), is very sensitive to different physical processes that may occur in the material, such as phase transitions or decomposition. In particular, we obtained values of the s parameter distributed around 0.5 for pure α-LAS and around 0.8 for α-LAS Yb 1.4 mol%, which were decreasing below 550 K (Figs. 12a and b). Apparently, a phase transition occurs in both compounds, becoming the paraelectric phase of the β-polymorphs. On cooling, the samples presented a completely disordered state (s = 0) between approximately 500 and 400 K, then a reordering process started in the crystal until room temperature was reached (Figs. 12a and b). Initially, there are no substantial differences between pure and doped compounds with an α-habit. By contrast, in the case of β-LAS, the s parameter varied between 0.7 and 0.8, from 200 to 250 K (Fig. 12c). However, a significant disorder between 250 and 290 K is observed (s = 0), at the interval of temperatures where the ferroelastic–ferroelectric phase transition occurs. This range includes the pre-transition showed in the curve of the complex permittivity (Figs. 9a and b). During the existence of the ferroelectric phase, the process became ordered (s = 1) around 340 K. At higher temperatures s is close to 1 until the next phase transition. At the ferroelectric–paraelectric transition, a significant disorder (s = 0.6) is observed; after that, the s parameter took values around 0.8. On cooling, during the paraelectric–ferroelectric transition the values of s remained around 0.9 (Fig. 12c). When the crystal returned to the ferroelectric phase, s became 1 again.

Figure 11
Frequency dependence of σ' at several temperatures, corresponding to the first heating cycles (298 → 550 K) for α-LAS Yb 1.4 mol% (top) and β-LAS (bottom) single crystals. The solid lines are the conductivity fits given by equation (1).

Figure 12
Temperature dependence of the s parameter, measured between 190 and 550 K in cycle 1 (on heating by red stars and on cooling by blue squares) for pure (a) α-LAS, (b) α-LAS Yb 1.4 mol% and (c) β-LAS single crystals. Vertical lines indicate the temperature for the ferroelastic–ferroelectric (black line) and ferroelectric–paraelectric (olive line) phase transitions, approximately.

research papers

4. Conclusions

The synthesis of LAS doped with Er^{3+} and Yb^{3+} had led us to obtain single crystals of the α-modification at temperatures between 298 and 313 K, instead of the more favorable and denser ferroelectric β-phase. When the ionic radius of the rare earth decreases, the substitution of the ammonium ion favors the more open layered structure. In particular, when Yb^{3+} is partially substituted, two new crystal structures: α_1- and α_2-LAS, have been determined by X-ray diffraction of single crystals. Both structures belong to the space group $P2_1/c$ and a displacive distortion has been calculated between them. Our two new structures show there are symmetry relations among layers and domains belonging to each layer, which are not completely described in the model proposed by Komornicka et al. (2014).

Moreover, we perform a comparative study between the α_1, α_2 polytypes of the α-type and the paraelectric and ferroelectric phases of the β-type. Although there are no symmetry operations relating them, we found a common structural motif that results in one of the lattice parameters having the same magnitude or a multiple thereof in both phases. The slight anomaly in the thermal dependence of the lattice parameters and the dielectric permittivity between 220 and 260 K in single crystals can be related with an intergrowth from the common axis between both phases.

The thermal dependence of diffractograms for polycrystalline samples and dielectric permittivity for single crystals, including an analysis of the order–disorder parameter s, reveals that the α-polytypes undergo an irreversible and reconstructive phase transition around 500 K to the paraelectric β-phase. Doped samples of α-polytypes remain stable between 200 and about 500 K.

Therefore, in this work, we have succeeded in clarifying most of the controversy on the stability of the α-polytypes. We have given information that helps explain the nature of the α-polytypes (with two new structures) and the key for explaining the reconstructive $\alpha \rightarrow \beta$ phase transition (through the common structural motif between both structural modifications). The enriched diversity of LiO_4 and SO_4 tetrahedra-based phases, built by chains, layers or three-dimensional connections, can serve for studies of the macroscopic symmetry lowering or/and changes in the $[LiSO_4]^-$ framework dimensionality and their current applications, for instance, ferroic phases, nonlinear and transport properties (Hlinka et al., 2016; Mishra et al., 2013).

References

Agilent (2014). *CrysAlisPro*. Agilent Technologies Ltd, Yarnton, Oxfordshire, England.

Aroyo, M. I., Perez-Mato, J. M., Orobengoa, D., Tasci, E., de la Flor, G. & Kirov, A. (2011). *Chem. Commun.* **43**, 183–197.

Belsky, A., Hellenbrandt, M., Karen, V. L. & Luksch, P. (2002). *Acta Cryst.* B**58**, 364–369.

Closser, R. G., Gualtieri, E. J., Newman, J. A. & Simpson, G. J. (2013). *Mater. Sci. Eng.* **46**, 1903–1906.

Czaja, P. (2013). *J. Therm. Anal. Calorim.* **113**, 91–95.

Dissado, L. A. & Hill, R. M. (1979). *Nature*, **279**, 685–689.

Gaffar, M. A. & Abu El-Fadl, A. (1999). *Physica B*, **262**, 159–169.

Guzmán-Afonso, C., González-Silgo, C., González-Platas, J., Torres, M. E., Lozano-Gorrín, A. D., Sabalisck, N., Sánchez-Fajardo, V., Campo, J. & Rodríguez-Carvajal, J. (2011). *J. Phys. Condens. Matter*, **23**, 325402.

Hlinka, J., Privratska, J., Ondrejkovic, P. & Janovec, V. (2016). *Phys. Rev. Lett.* **116**, 177602.

Itoh, K., Ishikura, H. & Nakamura, E. (1981). *Acta Cryst.* B**37**, 664–666.

Jonscher, A. K. (1977). *Nature*, **267**, 673–679.

Komornicka, D., Wołcyrz, M. & Pietraszko, A. (2014). *Cryst. Growth Des.* **14**, 5784–5793.

León, C., Lucía, M. L. & Santamaría, J. (1997). *Phys. Rev. B*, **55**, 882–887.

Lim, A. R. (2016). *Solid State Commun.* **247**, 23–26.

Lima, R. J. C., Sasaki, J. M., Ayala, A. P., Freire, P. T. C., Mendes-Filho, J., Melo, F. E. A., Ellena, J. & Santos Jr, S. (2003). *Acta Cryst.* C**59**, i67–i70.

Lim, A. R. & Kim, S. H. (2012). *Solid State Ionics*, **214**, 19–24.

Lv, W., Tong, Z., Yin, Y. M., Yin, J. & Ma, Z. (2015). *Nano-Micro Lett.* **7**, 268–275.

Maczka, M., Souza Filho, A. G., Paraguassu, W., Freire, P. T. C., Mendes Filho, J. & Hanuza, J. (2012). *Prog. Mater. Sci.* **57**, 1335–1381.

Mashiyama, H. & Kasano, H. (1993). *J. Phys. Soc. Jpn*, **62**, 155–162.

Mata-Ramírez, J. O. (2002). PhD thesis. University of Barcelona, Spain.

Mel'nikova, S. V., Kartashev, A. V., Grankina, V. A. & Flerov, I. N. (2003). *Phys. Solid State*, **45**, 1572–1578.

Mishra, A. K., Murli, C., Verma, A. K., Song, Y., Kumar, M. R. S. & Sharma, S. M. (2013). *J. Phys. Chem. A*, **117**, 5734–5741.

Ngai, K. L., Jonscher, A. K. & White, C. T. (1979). *Nature*, **277**, 185–189.

Orobengoa, D., Capillas, C., Aroyo, M. I. & Perez-Mato, J. M. (2009). *J. Appl. Cryst.* **42**, 820–833.

Palmero, I. C., González-Silgo, C., Torres, M. E., Marrero-López, D., Rivera-López, F., Haro-González, P. & Solans, X. (2008). *J. Lumin.* **128**, 1025–1028.

Pietraszko, A. & Lukaszewicz, K. (1992). *Pol. J. Chem.* **66**, 2057–2061.

Połomska, M. (2001). *Phase Transitions*, **74**, 409–468.

Połomska, M., Hilczer, B. & Baran, J. (1994). *J. Mol. Struct.* **325**, 105–110.

Połomska, M., Wolak, J. & Kirpichnikova, L. (2005). *Mater. Sci. Eng. B*, **120**, 76–83.

Ran Lim, A., Hyoun Kim, H. & Lee, M. (2013). *J. Solid State Chem.* **199**, 96–101.

Rodríguez-Carvajal, J. (1993). *Physica B*, **192**, 55–69.

Rousse, P. & Tarascon, J. M. (2014). *Chem. Mater.* **26**, 394–406.

Rudysh, M., Stadnyk, V., Brezvin, R. & Shchepanskii, P. (2015). *Phys. Solid State*, **57**, 53–58.

Shamshin, A. P. (2010). *Ferroelectrics*, **397**, 9–15.

Sheldrick, G. M. (2015). *Acta Cryst.* C**71**, 3–8.

Solans, X., Mata, J., Calvet, M. T. & Font-Bardia, M. (1999). *J. Phys. Condens. Matter*, **11**, 8995–9007.

Tomaszewski, P. E. (1992*a*). *Solid State Commun.* **81**, 333–335.

Tomaszewski, P. E. (1992*b*). *Phase Transitions*, **38**, 127–220.

Tomaszewski, P. E. (2000). *J. Phys. Condens. Matter*, **12**, 8933–8936.

Waśkowska, A. & Allmann, R. (1982). *Cryst. Struct. Commun.* **11**, 2029–2034.

Xiao, R., Li, H. & Chen, L. (2015). *J. Materiomics*, **1**, 325–332.